Using Landsat-5 TM and Field Data for Land Cover Classification and Terrestrial Carbon Stock Estimation Along the Kolyma River near Cherskiy, Russia

Dylan E. Broderick

MAY 2012

A THESIS

Submitted to the faculty of Clark University, Worcester, Massachusetts, in partial fulfillment of the requirements for Honors in the department of Geography

And accepted on the recommendation of

Karen Frey, Chief Instructor

ABSTRACT

Using Landsat-5 TM and Field Data for Land Cover Classification and Terrestrial Carbon Stock Estimation Along the Kolyma River near Cherskiy, Russia

Dylan E. Broderick

The objective of this study is to create a detailed land cover map for a 3036 km^2 region around Cherskiy in northeastern Russia using Landsat-5 Thematic Mapper data, and characterize the terrestrial carbon content of the study area based on field samples of soil and vegetation collected in July 2011. Field estimates of carbon (Mg ha^{-1}) were obtained for overstory, understory, and belowground (top 10 cm of soil) reservoirs at seven sites, which were broadly stratified as larch forest, floodplain, or shrubland. Land cover classification was performed on the Landsat data to derive six categories: bare soil, floodplain, larch, built, water, and shrubland. Maximum likelihood and minimum distance algorithms were evaluated using Worldview-2 imagery as reference data. Overall map accuracy for the minimum distance map was 82%, average commission error was 17%, and average omission error was 17%; in contrast, the maximum likelihood map had an overall accuracy of 76%, average commission error of 27%, and average omission error of 23%. Carbon estimations were made using spectral mixture analysis, which combined fraction images for floodplain, larch, and shrubland with field measurements of carbon stock for each class. The fraction images were summed to create total, aboveground, and belowground carbon maps. Results indicated that the floodplain regions contained the largest amount of carbon per ha, but made up the smallest area overall. The total estimated terrestrial carbon content for the study area was 12.59 Tg based on the high accuracy minimum distance map, with 4.96 Tg allocated aboveground and 7.63 Tg belowground.

Karen Frey, Ph.D.

Chief Instructor

John Rogan, Ph.D.

Assistant Professor

ACKNOWLEDGEMENTS

I thank my parents, Ray and Denise, and my sister, Sadie, for all of their support and encouragement both before and during my time at Clark University. I thank Professor Karen Frey for her enthusiasm and for inspiring me to pursue Arctic research, and Professor John Rogan for all I have learned about remote sensing. Finally, I thank all the students, professors, scientists, and affiliates of the Polaris Project 2011, especially Sam Dunn, Allison Stringer, and Professor Andy Bunn, for giving me the opportunity to learn, work, and play in the Russian Arctic.

TABLE OF CONTENTS

Introduction

Satellite imagery is often used to classify land cover types over large areas, such as the Arctic, and is useful for understanding the distribution, extent, and types of vegetation in relation to biogeochemical processes (Turner et al. 2004; Chen et al. 2009; Fuchs et al. 2009). Optical remote sensing can distinguish different vegetation types based on spectral characteristics and structural properties, and has been effectively employed to estimate the distribution of aboveground biomass (Krankina 2004; Turner et al. 2004; Barrett et al. 2009; Potapov 2011). Developing an understanding of overall land cover composition in vast, remote regions of the Arctic can help to determine current land cover patterns and potential land cover change, which is likely to occur with the predicted warming of 6 to 7^{o}C in northern latitudes by the end of the 21st century (IPCC 2007). Increased temperatures are projected to trigger the release of large amounts of carbon from organic matter stored in permafrost (Heikkinen et al. 2004; Frey and McClelland 2009; Fuchs et al. 2009). The release of accumulated permafrost carbon to the atmosphere is part of a positive feedback that is potentially large enough to influence local and global surface temperatures (Oechel and Vourlitis 1994). Siberia comprises the majority of land area in the Arctic; therefore, understanding its vegetation and soil dynamics, including carbon content, is instructive in predicting how climate change may impact terrestrial landscapes at high latitudes (Fuchs et al. 2008).

Several studies have combined satellite remote sensing and field data of carbon stocks to estimate carbon content or fluxes in Arctic regions of Canada, Alaska, and Russia (Hinkel et al. 2003; Krankina 2004; Sitch et al. 2007; Chen et al. 2009; Fuchs et al. 2009; Hugelius et al. 2010; Potapov 2011). Mapping land cover type is an important first step in understanding the spatial distribution of carbon stocks because different cover types vary in their ability to store carbon (Turner et al. 2004). Sitch et al. (2007) used 1 km Advanced Very High Resolution Radiometer

(AVHRR) data for Arctic tundra ecosystems from 1988 to 2002 to assess past trends in Normalized Difference Vegetation Index (NDVI) for Arctic vegetation, subsequent CO_2 and CH_4 exchange between the land and atmosphere, and future carbon fluxes that may occur with continued warming. The study concluded that Arctic will act as a sink for carbon over the next century but methane emissions will increase substantially, suggesting that tundra ecosystems will contribute to climate warming through the accelerated flux of greenhouse gases to the atmosphere. Chen et al. (2009) estimated rates of land use change in the Canadian Arctic and the resulting changes in CO_2 flux from 1985 to 1990 and from 1990 to 2000 using Landsat-5 and Japanese Earth Resources Satellite-1 (JERS-1) data, concluding that over time changes in land use patterns caused CO_2 flux to decline.

After classifying land cover from remotely sensed data, field measurements of carbon storage for particular cover types were used previously to estimate total carbon storage for a given region (see Barrett 2009; Chen et al. 2009; Fuchs et al. 2009; Potapov 2011). Hinkel et al. (2003) used Landsat-7 Enhanced Thematic Mapper+ (ETM+) imagery to classify land cover types, particularly drained lake basins, and then used soil cores from these basins to estimate their age and the soil organic carbon content for the Barrow Peninsula, Alaska. The results indicated that the organic layer thickness and decomposition rate tended to increase with basin age. Similarly, Fuchs et al. (2009) estimated mean aboveground carbon stock for a region in central Siberia using field measurements and Quickbird and Advanced Spaceborne Thermal Emission and Reflection Radiometer (ASTER) data, revealing high spatial variability in carbon content across the 45 ha study area. Although remote sensing satellites do not directly measure carbon, they are able to detect certain physical properties (such as aboveground vegetation composition and condition), which can be linked to carbon storage (Sitch et al. 2007).

Though there are many studies involving carbon estimation in Arctic landscapes using satellite imagery, most focus on aboveground or belowground storage separately, and do not combine these components to develop an estimation of overall terrestrial carbon stock (Golubyatnikov 2001; Hinkel et al. 2003; Sitch 2007; Hugelius et al. 2010; Potapov 2011). Additionally, studies estimating carbon content in the region around the Kolyma River and the city of Cherskiy in northeastern Russia are limited (Fuchs et al. 2009). The Kolyma River region is important to study because it is the largest Arctic river basin underlain by continuous permafrost, with substantial carbon stocks that could be released to the atmosphere with continued climate warming (Zimov et al. 2006). This study aims to provide a more comprehensive understanding of land cover types and carbon storage in northeastern Siberia that can be incorporated into more comprehensive analyses of the Arctic as a whole.

The objectives of this study are twofold. First, a land cover map was created to characterize the spatial extent and variation of six land cover types: bare soil, floodplain, larch forest, water, built, and shrubland. Second, terrestrial carbon content of the study area was estimated using field samples of carbon in biomass and the top 10 cm of the soil. These above and belowground carbon estimations were determined using field data measurements of carbon in 0.2 ha plots classified as floodplain, larch, or shrubland. The estimations were subsequently related to land cover types in the classification map and the fraction images produced using spectral mixture analysis (SMA) to extrapolate the total amount of carbon in the study area.

Study Area

The study area is approximately 3036 km^2 in size and is located in northeastern Siberia along the Kolyma River near the city of Cherskiy, Russia, at 68^o 45' N and 161^o 18' E, approximately 240 km north of the Arctic Circle (Figure 1). The region belongs to the

administrative region of Sakha Republic (formerly Yakutia) of the Russian Federation. Average temperatures range from -35^{o}C in January to 18^{o}C in July, and the annual precipitation average is approximately 1500 mm (NCDC 2012). The entire region is underlain with 350–650 m of continuous permafrost, and the depth of the active layer (the top layer of permafrost that thaws and refreezes each year) ranges from 0 cm in February to 20–50 cm in July (Walter et al. 2006; Schuur et al. 2008).

The deciduous needle-leaf species *Larix cajenderi* (Dahurian larch) is the dominant tree type of the region. Other vegetation types consist largely of shrub and understory species, including *Betula nana* (dwarf birch), *Pinus siberica* (dwarf pine), *Ledum palustre* (Labrador tea), and a variety of mosses and grasses (Kajimoto et al. 2006). Dominant soil types consist of entisols, gelisols, and loess deposits which make up yedoma soils, consisting of 50–90% ice (Kajimoto et al. 2006). Topography ranges from approximately 50 m to 500 m above sea level, though the majority of the region lies below 200 m (USGS 2011). The average slope is one degree and the average aspect is 180 degrees (west-facing). Higher elevations are found in the north and east of the study area, while the south and west are much flatter, with a large number of lakes ranging in size from 5 m to over 2000 m in diameter (USGS 2011). Streams and small rivers from the floodplain region feed into the northward flowing Kolyma River, which empties into the Arctic Ocean (USGS 2011). Settlement is sparse and minimal throughout the region, and Cherskiy is the largest city with a population of approximately 3700 (Federal State Statistics Service 2011).

Data and Methods

Satellite and ancillary data

A 30 m spatial resolution Landsat-5 Thematic Mapper (TM) image acquired on 11 July 2011 was used to map land cover in the study area (row 12, path 105; Figure 1). The image was 100% cloud-free and corresponded to the same time period that field measurements were made. Atmospheric correction was performed using dark object subtraction, which subtracts non-zero pixel values for dark objects from all other pixels in the image to remove atmospheric scattering effects (Chavez 1996). Ancillary data include a Northern Circumpolar Soils Map from the National Snow and Ice Data Center (NSIDC; Tarnocai et al. 2002), a Northern Eurasia Landcover Map with 29 categories and 1 km spatial resolution from Global Environmental Monitoring (GEM; Bartelev et al. 2003), and a digital elevation model (DEM) and streams layers from the USGS Hydro1K dataset for Asia, both with a 1 km spatial resolution (USGS 2011). Panchromatic Worldview-2 imagery (0.5 m) acquired on 28 August 2011 and visual field observations made during sampling regarding vegetation types and density, topography, and water bodies in and around each plot were used as a reference in the visual and quantitative assessments of map accuracy.

Field data collection

Figure 2 provides an overview of the methodological steps taken using the field measurements and remote sensing techniques. Estimations of carbon content in soil and vegetation were made at seven circular field sites, each 0.2 ha in diameter (Table 1). The locations of field measurements were recorded with a Magellan Triton 1500 GPS system with an average positional accuracy of 4 m. Four plots were located in larch dominated forests, two in shrubland regions (one low-lying elevation of approximately 43 m and one at a higher elevation

of approximately 113 m), and one in a floodplain (Figure 1). For all trees in each plot, diameter at breast height (DBH), defined as 1.4 m from the base of the tree, was measured and used to determine above- and below-ground carbon of the tree using published allometric relationships developed to assess biomass allocation in larch trees of northeastern Siberia (Kajimoto et al. 2006):

$$y = A * DBH^{B} \quad (1)$$

where y is dry mass in kg, A is a proportionality coefficient, and B is the scaling exponent. DBH of snags (standing dead trees) and coarse woody debris (fallen dead trees) was also measured within the plot. These measurements constituted the overstory component of carbon stock for each site.

Understory carbon measurements were based on ground-cover. Percent cover within a quadrat (1 m), placed 15.8 m from the center of the plot (as per sampling protocol) along north, south, east, and west transects, was estimated and recorded. Cover types included shrubs, vaccinium, fine woody debris, moss, and Labrador tea. Additionally, all groundcover within the quadrat along the north transect of the plot was clipped, sorted into the above categories, and weighed. Subsamples of each cover type were dried in a drying oven for 24 hours, weighed, and combusted at 450^{o}C for 24 hours to measure loss of carbon on ignition (LOI). The difference in weight before and after combusting was assumed to be the organic carbon content of the sample (modified from Reeuwijk 2002). Estimates of grams of carbon per gram of vegetation, based on average percent cover from other transects within the plot, were used to calculate total groundcover (and therefore carbon content) for the entire plot (Fuchs et al. 2008).

Belowground carbon was measured by taking two 10 cm soil samples using a soil auger with a one cm diameter from within the quadrat used for understory estimates along the north, south, east, and west transects. As with understory samples, soil samples were weighed, dried for 24 hours, and combusted for 24 hours at 450^{o}C to measure LOI and estimate belowground carbon in the top 10 cm of soil for the entire plot (Reeuwijk 2002). Belowground carbon also included the root component of carbon estimation for vegetation based on the allometric equations from Kajimoto et al. (2006). Total carbon for each plot type was calculated by adding overstory, understory, and belowground components, and was expressed in terms of megagrams of carbon per hectare (Mg ha^{-1}) (Table 1).

Land cover classification

Two supervised classifications, minimum distance and maximum likelihood (Figures 3), were performed to classify land cover types using the pre-processed Landsat data and determine which classification algorithm was more spatially accurate for this application. Six land cover types were defined for classification: bare soil and rock, floodplain (marsh regions bordering lakes and rivers that are prone to flooding), larch forest (consisting of 75–100% larch trees), urban and built (cities, towns, roads, and infrastructure), water, and shrubland (low-lying woody and non-woody vegetation). The classes were selected to be exhaustive and to correspond with the categorization of the field sites as larch forest, floodplain, or shrubland during the collection of field data.

Training sites were digitized from a false infrared composite of Landsat band 4 (red), band 3 (green), and band 2 (blue) using visual inspection, field observations of each site, Google Earth imagery from 2009 (Google Earth 2011), Worldview 2 imagery from August 2011, and

ancillary land cover maps to assign pixels to each of the six classes. Training sites were selected across the entire study area and contained the following number of pixels per site: 3957 for bare soil and rock; 5233 for floodplain; 9094 for larch; 2204 for built; 97658 for water; and 14428 for shrubland. Outputs from these classifications were compared with field observations of each site and ancillary land cover maps to assess which was deemed more accurate qualitatively with regard to landscape characteristics. Quantitative accuracy assessment was performed for both supervised outputs using panchromatic 0.5 m spatial resolution WorldView-2 imagery, acquired on 28 August 2011, as the validation imagery (Figure 4). Stratified random sampling was used to create independent training sites for validation image (30 per land cover category). The training sites were compared to the maximum likelihood and minimum distance maps to determine map accuracy.

Biomass and carbon estimation

The total area of floodplain, larch, and shrubland regions within the study area was calculated based on the hard classification outputs. This involved multiplying the total area of each cover type by the corresponding field measurement of carbon (Mg ha^{-1}) to provide an overall estimation of carbon content per vegetation class across the study area. Values were converted to grams per square meter (g m^{-2}) to be consistent with other studies quantifying carbon storage across large regions.

Spectral mixture analysis (SMA) was also performed on the Landsat data to provide more precise, continuous estimates of floodplain, larch, and shrubland areas by considering the relative percentage of each cover type within a pixel. Image endmembers were defined for floodplain, larch, and shrubland by selecting training sites of 20 pixels that were exclusive; that is, they were comprised entirely of one cover type with no mixture of the other vegetation classes (see Figure

4 for examples of pure endmembers). SMA produced four fraction images, three of which displayed the proportion of each vegetation type within each pixel, and a fourth residual image (Figure 5). The class-specific images were multiplied by the total, aboveground, and belowground carbon estimates for their respective cover types, which had been converted into units of Mg per pixel. The pixel values from each vegetation-specific carbon map were then summed to yield total, aboveground, and belowground carbon maps, and units were converted to g m^{-2}. Finally, the values from each of the three carbon map were summed to provide numerical estimates of carbon in the study area in teragrams (Tg).

Results

Field results

Field measurements revealed general distinctions in the allocation of carbon between the overstory, understory, and belowground components for the larch forest, floodplain, and shrubland sites (Table 1). The majority of carbon was allocated belowground for all three sites, but it was much higher in the floodplain region owing to relatively high rates of productivity, decomposition, and nutrient deposition associated with wetland soils (Hinkel et al. 2003; Hugelius et al. 2010) (Figure 6). Distribution of carbon in larch forests differed by 0.75 Mg between overstory and understory components, while the understory component was 3.15 Mg and 18.65 Mg larger in floodplain and shrubland regions, respectively. The floodplain region had the greatest amount of terrestrial carbon storage (64.15 Mg ha^{-1}), followed by larch forest (52.97 Mg ha^{-1}) and shrubland (43.23 Mg ha^{-1}). The aboveground to belowground carbon ratios were 0.05 for floodplain, 0.91 for larch, and 0.83 for shrubland (Table 1).

Land cover classification

The maximum likelihood and minimum distance supervised classifications were similar in appearance, but the maximum likelihood map appeared less accurate conceptually based on the topography and hydrology of the study area (Figure 3b). Regions of disagreement between the two maps were compared with ancillary data including additional land cover maps, the DEM, Google Earth imagery, Worldview 2 imagery, and visual field observations from each site. The majority of disagreement occurred along edges of classes, particularly among the floodplain and larch regions. Classes with the greatest areal difference between the maximum likelihood and minimum distance maps were bare soil (55788 ha) and floodplain (27739 ha) regions. The land cover classes with the smallest areal difference between maps were built (190 ha) and water (1369 ha), as these categories have more distinct spectral signatures and therefore were less susceptible to confusion during classification.

After comparing the supervised classification outputs with the ancillary data including the DEM (USGS 2011), field observations of the study area, and the GEM land cover map (Bartelev et al. 2003), it was deemed that the minimum distance classification was visually more accurate and should therefore be used as the classification image. This was confirmed with a quantitative accuracy assessment using independent training sites for each map and WorldView-2 validation imagery (Table 2). For each land cover category, 30 ground reference points were identified in the Worldview-2 imagery and then were compared with the minimum distance and maximum likelihood outputs to determine the level of agreement. The overall accuracy for the minimum distance map was 82%, average omission error was 17%, and average commission error was 20% (Table 2a). For the maximum likelihood map, overall accuracy was 76%, average omission error was 23%, and average commission error was 27% (Table 2b). Categories

showing the greatest difference between training sites for each map and the reference imagery were bare soil, floodplain, and shrubland. The maximum likelihood algorithm tended to overestimate floodplain, larch, and bare soil, while underestimating shrubland, because pixels with a reflectance that does not easily fall into a defined class (based on training sites) are awarded to the class with the larger area. Though the minimum distance map was considered more accurate, both hard classification outputs also have approximately 27 m of inherent positional error associated with the study owing to the relationship between the smallest objects being mapped, in this case tree crowns and small lakes (approximately 3 m), and the spatial resolution of the Landsat-5 imagery (30 m).

Carbon estimation

The minimum distance map classified 112191 ha of the study area as larch forest, 17746 ha as floodplain, and 116951 ha as shrubland. SMA mixture analysis produced fraction images of the proportion of each vegetation type in areas that were not classified as bare soil, built, or water, and these images were multiplied by the respective carbon stock for each class (Figure 5). Combining the fraction images yielded carbon maps for aboveground, belowground, and total carbon in the study area (Figure 7). After all pixel values for these three maps were summed converted to Tg, the total terrestrial carbon content for the entire study area (combined above and belowground components) was estimated to be 12.59 Tg, with 2.24 Tg in floodplains, 6.49 Tg in larch forests, and 3.87 in shrublands (Table 3). The total aboveground carbon component was estimated to be 4.96 Tg, while the belowground component was 7.63 Tg. A map of the aboveground to belowground carbon ratio was also created based on the SMA outputs of above and belowground stocks (Figure 7d).

Discussion and Conclusions

The field measurements indicate that in floodplain, larch, and shrubland regions, the greatest amount of carbon is stored belowground compared to the overstory and understory, even when only the top 10 cm of the soil is being measured (Tables 1 and 3). The belowground component, consisting of plant root material and soil, therefore represents an important potential source of carbon to the atmosphere, particularly with thawing permafrost that could trigger the release of this carbon (Zimov et al. 2006; Schuur et al. 2008; Frey and McClelland 2009). Floodplain regions likely had the greatest amount of belowground carbon owing to the transport and deposition of dissolved and particulate carbon by rivers which then accumulated in the soil (Meybeck 1993; Hinkel et al. 2003) (Figures 6 and 7c). Larch forest had a larger overstory carbon stock than floodplain and shrubland because of the presence of trees, which act as important carbon sinks (Krankina 2004) (Figures 6 and 7b). The reduced number or complete absence of trees in shrubland and floodplain regions, respectively, can be attributed to their low overstory carbon stock.

The minimum distance map classifies the majority of the study area as larch and shrubland, which is consistent with the land cover map from GEM and the WorldView-2 imagery (Figure 3a). The classification was successful in identifying water bodies, urban areas, and bare soil regions, which mainly occurred in areas of high elevation. Floodplain regions were also conceptually consistent, which were found primarily along the edges of lakes, rivers, and low-lying areas. The maximum likelihood classification was less accurate in this regard, often classifying bare soil regions adjacent to floodplains; based on topography and hydrology, this relationship between cover types is unlikely (Figure 3b).

Carbon estimation indicated that larch forest has the largest carbon storage of the three cover types analyzed (Figure 8). Although floodplain regions contain the greatest amount of carbon per ha, they make up the smallest percentage of the study area relative to larch forest and shrublands. These findings are consistent with those from other studies estimating carbon in the Arctic using remote sensing. Hugelius et al. (2010) concluded that there is substantial spatial variability in above and belowground carbon allocation between forests and wetlands, which store 20–30% and less than 1% of carbon in vegetation, respectively. The average aboveground carbon stock across all three vegetation types for this study is 16.01 Mg ha^{-1} (Table 1), which is in relatively close to the estimation by Fuchs et al. (2009) in central Siberia that showed 15.3 Mg ha^{-1} of aboveground carbon. Differences in estimations of carbon between studies are likely a result of field methods, image processing classification, and the spatial and temporal variability. Finally, the accuracy of 82% obtained for the minimum distance map in this study is lower than, but close to, the accuracy of 89% obtained by Potapov (2011), who used supervised classification and Landsat imagery to map forest cover in western Russia. Though the overall accuracy for this study falls below the commonly accepted accuracy threshold of 85% for land cover mapping, the overall accuracy of the map output should also be considered in terms of logical consistency, the accuracy achieved in similar studies, and imagery used for calibration and validation (Anderson et al. 1976).

The use of SMA allowed for a sub-pixel estimation of the percentage of each vegetation type across the study area, ultimately producing a soft classification of cover types and carbon quantities, in contrast to the hard classification created using the minimum distance algorithm (Figures 3a and 7). This methodology has been used to map aboveground biomass in other regions, such as the United States and the Amazon (Huang et al 2009; Asner 2010), but studies

in the Arctic that integrate above and belowground carbon with SMA are less common. SMA provides areal estimates of biophysical properties on the ground, making it a powerful classification method when combined with quantitative field measurements of carbon because of its relatively higher precision. In this study, the carbon quantities applied to the vegetation-specific fraction images include both above and belowground carbon measurements based on the field data, demonstrating how SMA can be used to calculate belowground carbon in addition to mapping aboveground biomass, as seen in previous studies (Figures 5 and 7).

This study addresses gaps in the research by quantifying above and belowground carbon stocks along Kolyma River and around the city of Cherskiy. A land cover map for the region was created, indicating the relative abundance of different cover types. Vegetation and soil carbon estimates were combined to provide a more comprehensive estimate of total carbon content, which is important when considering potential biogeochemical responses to increasing surface and atmospheric temperatures. Carbon estimations for this region of the Arctic can be compared to estimations for other Arctic landscapes to assess which areas may be the most vulnerable to warming or which areas will potentially release the largest amount of carbon. Additionally, differences in carbon stock across regions of the Arctic may imply different responses to warming related to hydrology, biodiversity, and primary productivity. Findings will also allow for comparisons of biogeochemical interactions, particularly carbon cycling, between this region and regions in other studies (Oechel and Vourlitis 1994; Lobbes et al. 2000; Krankina 2004; Fuchs et al. 2008; Chen et al. 2009).

Increasing the number of field sites for all three cover types, particularly floodplain regions, will strengthen and improve the findings of this study. Owing to time and accessibility constraints, it was not possible to collect more field data. The broad categorization of land cover

types, chosen to correspond with the field data, is another limitation that oversimplifies the estimation of carbon. Finally, this research assumes that each land cover type stores the same amount of carbon across the entire study area, while samples were taken from much smaller plots within relatively close proximity. This generalization is an inherent component of scaling individual site measurements to the regional level, and can only provide an approximate estimate of carbon content. A stratified random sampling design that collects field measurements across a larger area would help address this problem.

Future work will increase the number of field sites over a larger area to provide a better representation of variability in carbon storage across the landscape. The number of field sites per land cover category and the number of vegetation categories will also be expanded to create a more precise and specific estimate of carbon storage. Finally, a more comprehensive, empirical classification method, such as a decision tree classifier, will be used instead of deterministic methods in order to directly incorporate other landscape variables such as topography, hydrology, and existing land cover maps, which will hopefully improve the accuracy of the classification.

References

Anderson, J. R.; Hardy, E. E.; Roach, J. T.; and Witmer, R. E. 1976. A land use and land cover classification system for use with remote sensing data. U.S. Geological Survey Professional Paper 964. U.S. Geological Survey: Reston, VA.

Asner, G. P.; Powell, G. V. N.; Mascaro, J.; Knapp, D. E.; Clark, J. K.; Jacobson, J.; Kennedy-Bowdoin, T.; Balaji, A.; Paez-Acosta, G.; Victoria, E.; Secada, L.; Valqui, M.; and Hughes, R. F. 2010. High-resolution forest carbon stocks and emissions in the Amazon. *Proceedings of the National Academy of Sciences* 107(38):16732–37.

Barrett, K.; Rogan, J.; and Eastman, R. 2009. A case study of carbon fluxes from land change in the Southwest Brazilian Amazon. *Journal of Land Change Science*. 4(4):233–48.

Bartalev, S. A.; Belward, A. S.; Erchov, D. V.; Isaev, A. S.; Bartholomé, E.; Gond, V.; Vogt, P.; Achard, F.; Zubkov, A. M.; Mollicone, D.;Savin, I. Y.; Fritz, S.; Repina, G.; and Hartley, A. 2003. The Land Cover Map for Northern Eurasia for the Year 2000. GLC2000 database, European Commission Joint Research Centre, 2003.

Chavez, P. S. J. 1996. Image-based atmospheric corrections—Revisited and improved. *American Society for Photogrammetry and Remote Sensing* 62(9):1025–36.

Chen, W.; Blain, C.; Li, J.; Fraser, R.; Zhang, Y.; Leblanc, S.; Koehlaer, K.; Olthof, I.; Wang, J.; and McGovern, M. 2009. Estimating carbon release cause by land use changes over Canada's north during 1985-1990 and 1990-2000 using satellite Earth observation. *Journal of Geophysical Research*. 114.

Federal State Statistics Service. 2011. "Preliminary results of the 2010 all-Russian population census." 2010 All-Russian Population Census. Available online: http://www.perepis-2010.ru/results_of_the_census/results-inform.php. Accessed 24 April 2012.

Frey, K. E., and McClellend, J. W. 2009. Impacts of permafrost degradation on arctic river biogeochemistry. *Hydrological Processes* 23:169–82.

Fuchs, H.; Magdon, P.; Kleinn, C.; and Flessa, H. 2008. Estimating aboveground carbon in a catchment of the Siberian Forest tundra: Combining satellite imagery and field inventory. *Remote Sensing of Environment*. 113:518–31.

Golubyatnikov, L. L. 2001. Response of the net primary production to climate change for the European Russia. *Izvestiya Akademii: Nauk, Seriya Geograficheskaya.* 6:42–50.

Google Earth. 2012. Cherskiy, Russia. 68°44'59.91" N and 161°19'38.52" E. 15 September 2009. Accessed 23 April 2012.

Griffin, C. G.; Frey, K. E.; Rogan, J; and Holmes, R. M. 2011. Spatial and interannual variability of dissolved organic matter in the Kolyma River, East Siberia, observed using satellite imagery. *Journal of Geophyiscal Research*. 116: G03018.

Heikkinen, J. E. P.; Virtanen, T.; Huttunen, J. T.; Elsakov, V.; and Martikainen, P. J. 2004. Carbon balance in East European tundra. *Global Biogeochemical Cycles.* 18.

Hinkel, K. M.; Eisner, W. R.; Bockheim, J. G.; Nelson, F. E.; Peterson, K. M.; and Dai, X. 2003. Spatial extent, age, and carbon stocks in drained thaw lake basins on the Barrow Peninsula. *Arctic, Antarctic, and Alpine Research*. 35(3):291–300.

Hugelius, G., Kuhry, P., Tarnocai, C., and Virtanen, T. 2010. Soil organic carbon pools in a periglacial landscape: A case study from the central Canadian Arctic. *Permafrost and Periglacial Processes*. 21:16–29.

Huang, C.-Y.; Asner, G. P.; Martin, R. E.; Barger, N. N.; and Neff, J. C. 2009. Multiscale analysis of tree cover and aboveground carbon stocks in pinyon-juniper woodlands. *Ecological Applications* 19(3):668–81.

Intergovernmental Panel on Climate Change (IPCC). 2007. Working Group I: The physical science basis of climate change. *ARA 4 Report, Observations 4: Changes in Snow, Ice, and Frozen Ground*. Available online: http://ipcc-wg1.ucar.edu/wg1/wg1-report.html. Accessed 4 April 2012.

Kajimoto, T.; Matsuura, Y.; Sofronov, M. A.; Volokitina, A. V.; Mori, S.; Osawa, A.; and Abaimov, A. P. 1999. Above- and belowground biomass and net primary productivity of a *Larix gmelinii* stand near Tura, central Siberia. *Plant Soil* 255:281–92.

Kajimoto, T.; Matsuura, Y.; Osawa, A.; Abaimov, A. P.; Zyryanova, O. A.; Isaev, A. P.; Yefremov, D. P.; Mori, S.; and Koike, T. 2006. Size-mass allometry and biomass allocation of two larch species growing on the continuous permafrost region in Siberia. *Forest Ecology and Management* 222:314–325.

Krankina, Olga N. 2004. Carbon stores, sinks, and sources in forests of northwestern Russia: Can we reconcile forest inventories with remote sensing results? *Climatic Change* 67(2-3):257–72.

Lobbes, J.; Fitznar, H. P.; and Kattner, G. 2000. Biogeochemical characteristics of dissolved and particulate organic matter in Russian rivers entering the Arctic Ocean. *Geochimica et Cosmochimica Acta*. 64(17):2973–83.

Meybeck, M. 1993. Riverine transport of atmospheric carbon: Sources, global typology, and budget. *Water, Air, and Soil Pollution*. 70:443–63.

NCDC. 2012. "Global Summary of the Day." Station Cherskij. NNDC Climate Data Online: National Climatic Data Center. Available online: http://www.ncdc.noaa.gov/oa/climate/onlineprod/drought/xmgr.html. Accessed 4 April 2012.

Oechel, W. C. and Vourlitis, G. L. 1994. The effects of climate change on land—atmosphere feedbacks in Arctic tundra regions. *Trends in Ecology and Evolution* 9(9):324–29.

Potapov, P. 2011. Regional scale boreal forest cover and change mapping using Landsat composites for European Russia. *Remote Sensing of Environment* 155(2):548–61.

Potere, D. 2008. The horizontal positional accuracy of Google Earth's high resolution imagery archive. *Sensors* 8:1–10.

Reeuwijk, L. P. 2002. Procedures for Soil Analysis. Technical Paper. International Soil Reference and Information Center. Wageningen, The Netherlands.

Schuur, E. A. G.; Bockheim, J.; Canadell, J. G.; Euskirchen, E.; Field, C. B.; Goryachkin, S. V.; Hagemann, S.; Kuhry, P.; Lafleur, P. M.; Lee, H.; Mazhitova, G.; Nelson, F. E.; Rinke, A.; Romanovsky, V. E.; Shikolmanov, N.; Tarnocai, C.; Venevsky, S.; Vogel, J. G.; and Zimov, S. A. 2008. Vulnerability of permafrost carbon to climate change: Implications for the global carbon cycle. *Bioscience* 58(8):701–14.

Sitch, S.; McGuire, A. D.; Kimball, J.; Gedney, N.; Gamon, J.; Engstrom, R.; Wolf, A.; Zhuang, Q.; Clein, J.; and McDonald, K. C. 2007. Assessing the carbon balance of circumpolar arctic tundra using remote sensing and process modeling. *Ecological Applications* 17(1):213–34.

Tarnocai, C.; Kimble, J. M.; Swanson, D.; Goryachkin, S.; Naumov, Y. M.; Stolbovoi, V.; Jakobsen, B.; Broll, G.; Montanarella, L.; Arnoldussen, A.; Arnalds, O.; and Yli-Halla, M. 2002. *Northern Circumpolar Soils.* 1:10,000,000 scale map. Ottawa, Canada: Research Branch, Agriculture and Agri-Food Canada.

Turner, D. P.; Ollinger, S. V.; and Kimball, J. S. 2004. Integrating remote sensing and ecosystem process models for landscape to regional scale analysis of the carbon cycle. *Bioscience*. 54(6):573–84.

USGS. 2011. Hydro 1K Asia. Earth Resources Observation and Science (EROS) Center. Available online: http://eros.usgs.gov/#/Find_Data/Products_and_Data_Available/gtopo30/hydro/asia. Accessed 4 April 2012.

Walter, K., Zimov, S., Chanton, J., Verbyla, D., and Chapin III, F. 2006. Methane bubbling from Siberian thaw lakes as a positive feedback to climate warming: *Nature* 443:71–75.

Zimov, S. A.; Davydov, S. P.; Zimova, G. M.; Davydova, A. I.; Schuur, E. A. G.; Dutta, K.; and Chapin, F. S. 2006. Permafrost carbon: Stock and decomposability of a globally significant carbon pool. *Geophysical Research Letters* 33:L20502.

Tables

Table 1: Overstory, understory, belowground, and total carbon content for floodplain, larch, and shrubland cover types based on seven field plots.

Cover type	Overstory Carbon (Mg/ha)	Understory Carbon (Mg/ha)	Belowground Carbon (Mg/ha)	Total Carbon Stock (Mg/ha)	Aboveground/Belowground Carbon
Floodplain	0	3.15	60.99	64.15	0.05
Larch	12.25	13.01	27.71	52.97	0.91
Shrubland	0.49	19.14	23.60	43.23	0.83

Table 2a: Confusion matrix for minimum distance map and WorldView-2 validation map

		WorldView-2 Validation Map						Total	User's Accuracy	Commission Error
		Bare Soil	Floodplain	Larch	Water	Built	Shrub			
Minimum Distance Map	Bare Soil	24	0	0	0	6	0	30	60%	40%
	Floodplain	0	26	0	1	0	1	28	65%	35%
	Larch	0	6	38	0	0	4	48	95%	5%
	Water	0	0	0	39	0	0	39	85%	15%
	Built	8	0	0	0	34	0	42	88%	13%
	Shrubland	8	8	2	0	0	35	53	88%	13%
Total		40	40	40	40	40	40	240		
Producer's Accuracy		80%	93%	79%	100%	81%	66%			
Omission Error		20%	7%	21%	0%	19%	34%			

Table 2b: Confusion matrix for maximum likelihood map and WorldView-2 validation map

		WorldView-2 Validation Map						Total	User's Accuracy	Commission Error
		Bare Soil	Floodplain	Larch	Water	Built	Shrub			
Maximum Likelihood Map	Bare Soil	21	1	0	0	6	1	29	53%	48%
	Floodplain	1	27	3	2	0	3	36	68%	33%
	Larch	0	4	32	0	0	5	41	80%	20%
	Water	0	0	1	38	0	0	39	85%	15%
	Built	9	0	0	0	34	0	43	78%	23%
	Shrubland	9	8	4	0	0	31	52	78%	23%
Total		40	40	40	40	40	40	240		
Producer's Accuracy		72%	75%	78%	97%	79%	60%			
Omission Error		28%	25%	22%	3%	21%	40%			

Table 3: Carbon content in Tg per vegetation type for total, aboveground, and belowground components across the entire study area, based on SMA outputs.

	Estimated Carbon Content (Tg)		
Vegetation Type	Above	Below	Total
Floodplain	0.11	2.13	2.24
Larch	3.09	3.39	6.49
Shrubland	1.76	2.11	3.87
Entire study area	4.96	7.63	12.59

Figures

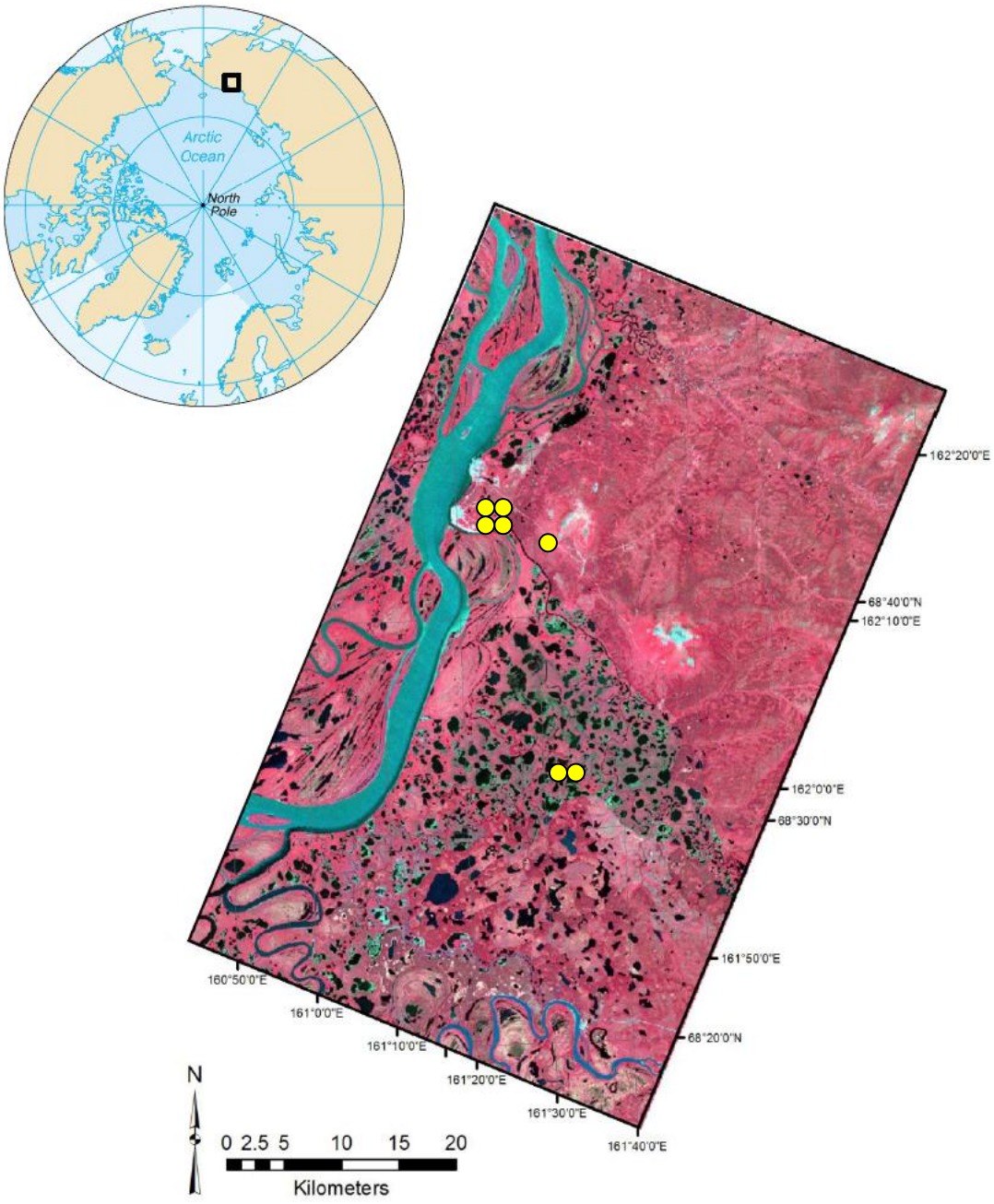

Figure 1: Study area with the seven field site locations shown in yellow.

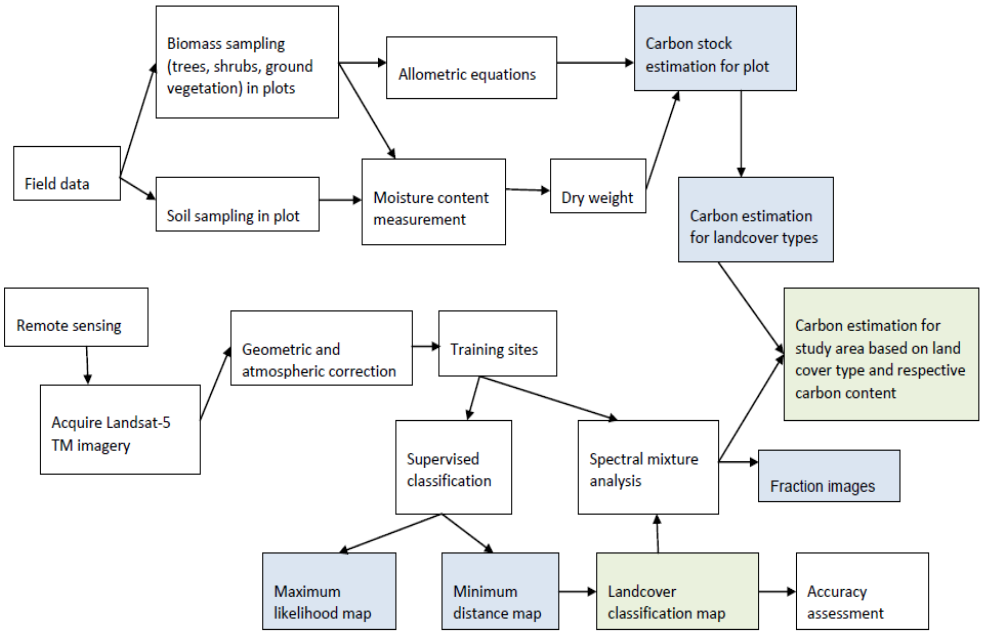

Figure 2: Flow chart of input data, methodology, and outputs used in the analysis (intermediate outputs in blue, final outputs in green).

a. 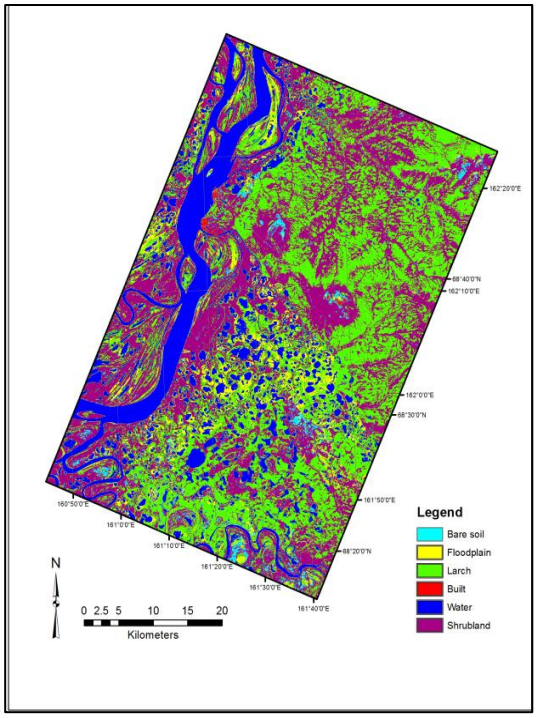

b. 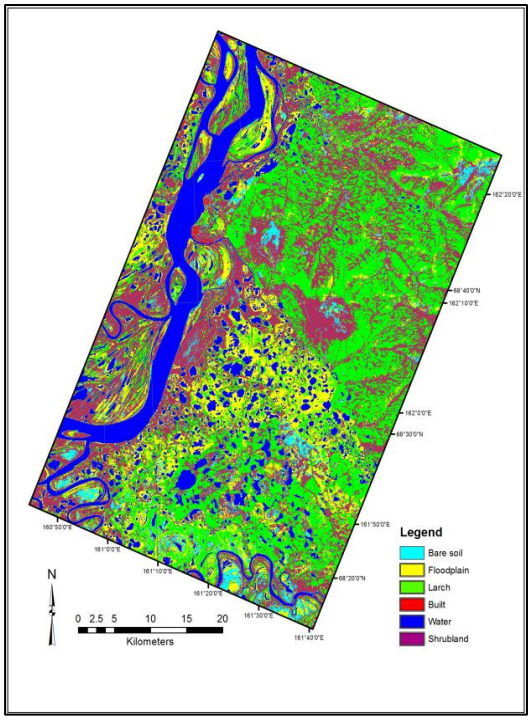

Figure 3: Minimum distance (a) and maximum likelihood (b) classification outputs for land cover types across the study area.

a.  b. 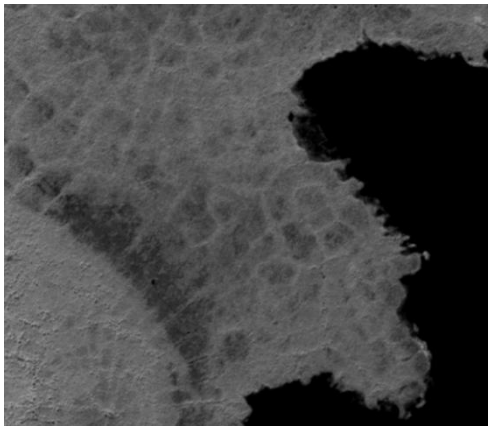

c. 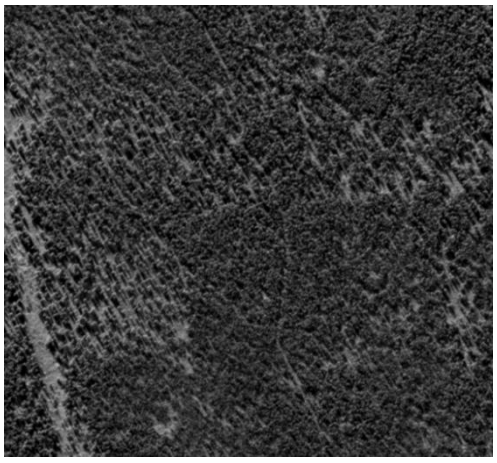 d. 

e. 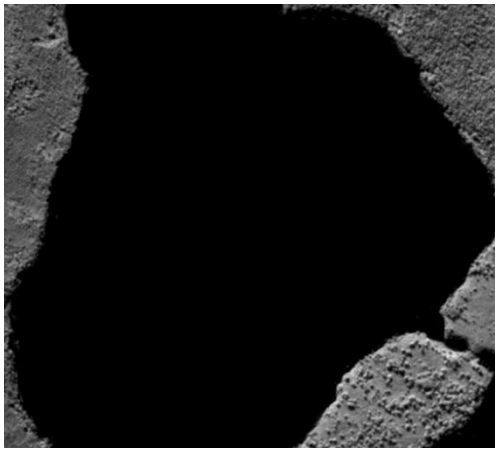 f. 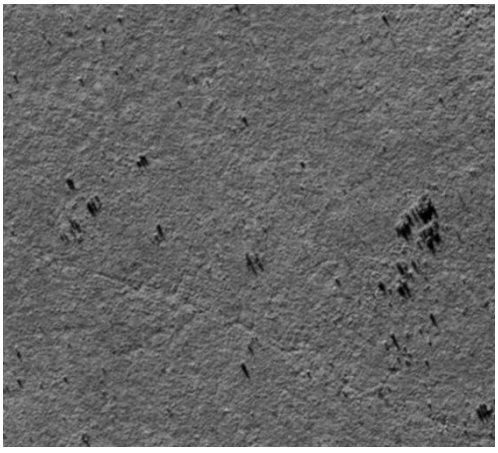

Figure 4: Examples of six cover types as seen with Worldview 2 imagery, which was used as a guide to designate training sites and to perform the accuracy assessment: (a) bare soil, (b) floodplain, (c) larch, (d) built, (e) water, and (f) shrubland.

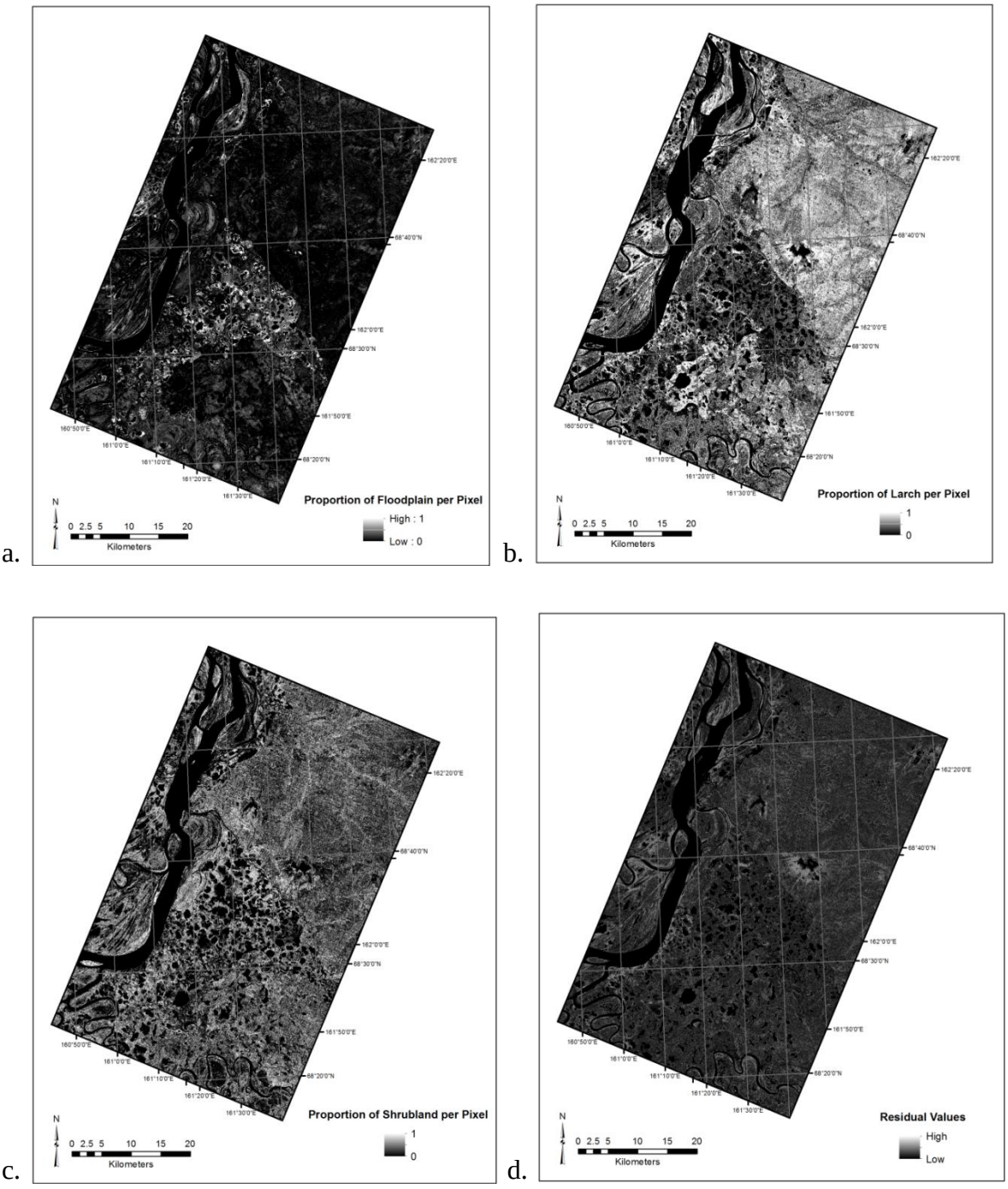

Figure 5: Spectral mixture analysis fraction images for floodplain (a), larch (b), shrubland (c), and residuals (d).

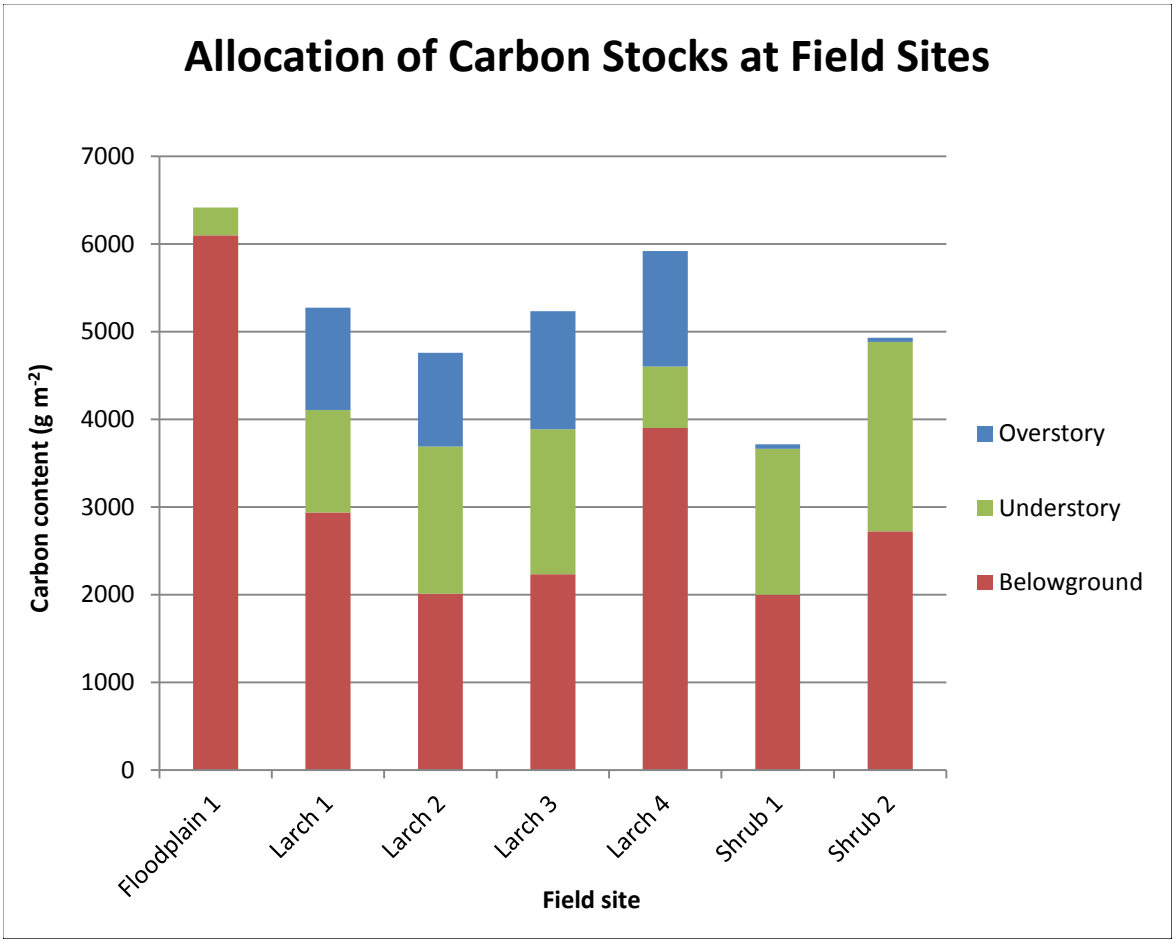

Figure 6: Allocation of carbon content measured in the overstory, understory, and belowground (top 10 cm) components for seven 0.2 ha field sites consisting of floodplain, larch, and shrubland cover types.

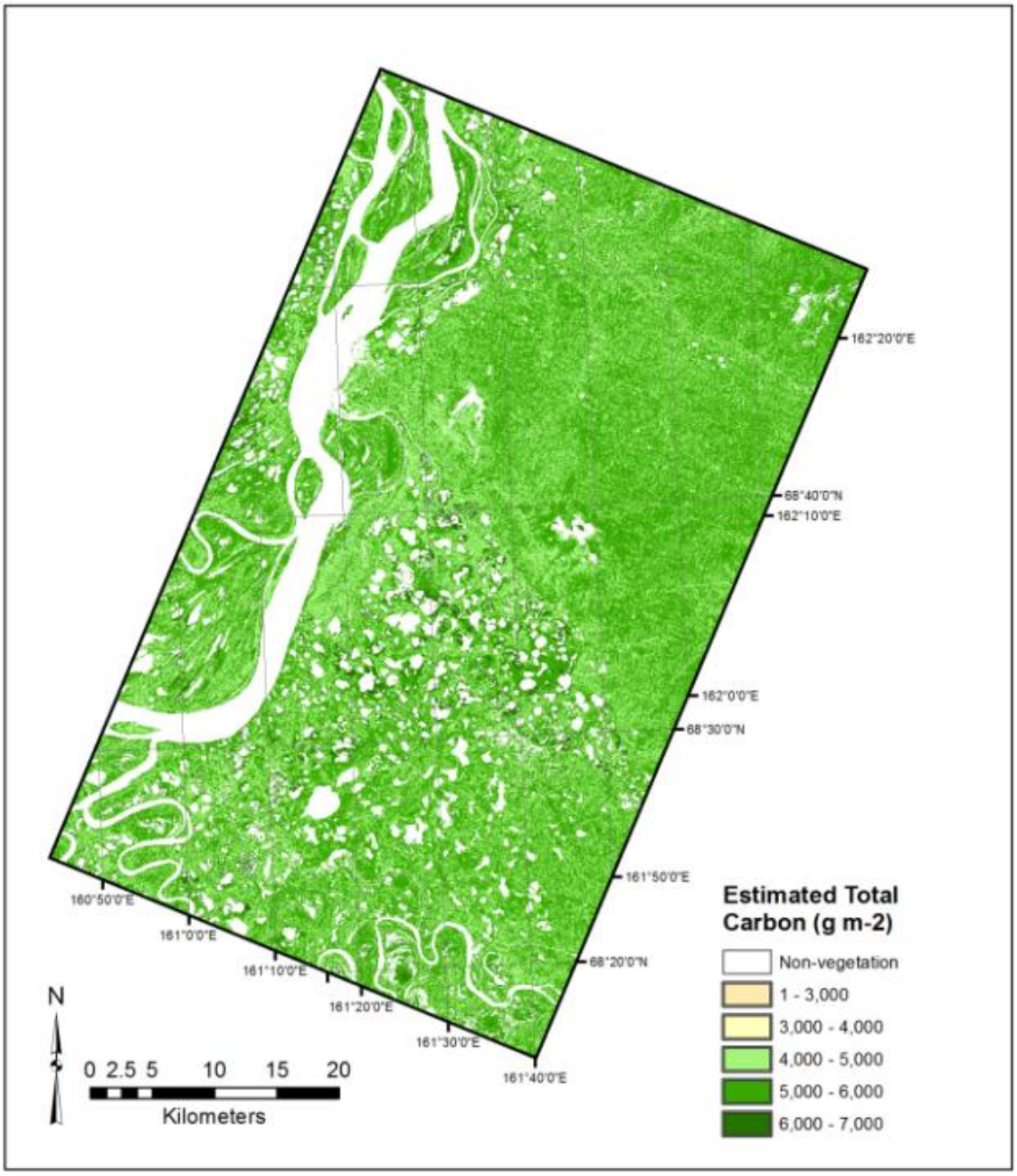

Figure 7a: Spectral mixture analysis output estimating the total carbon in g m^{-2} based on the relative proportion of floodplain, larch, and shrubland and the measured carbon content associated with each.

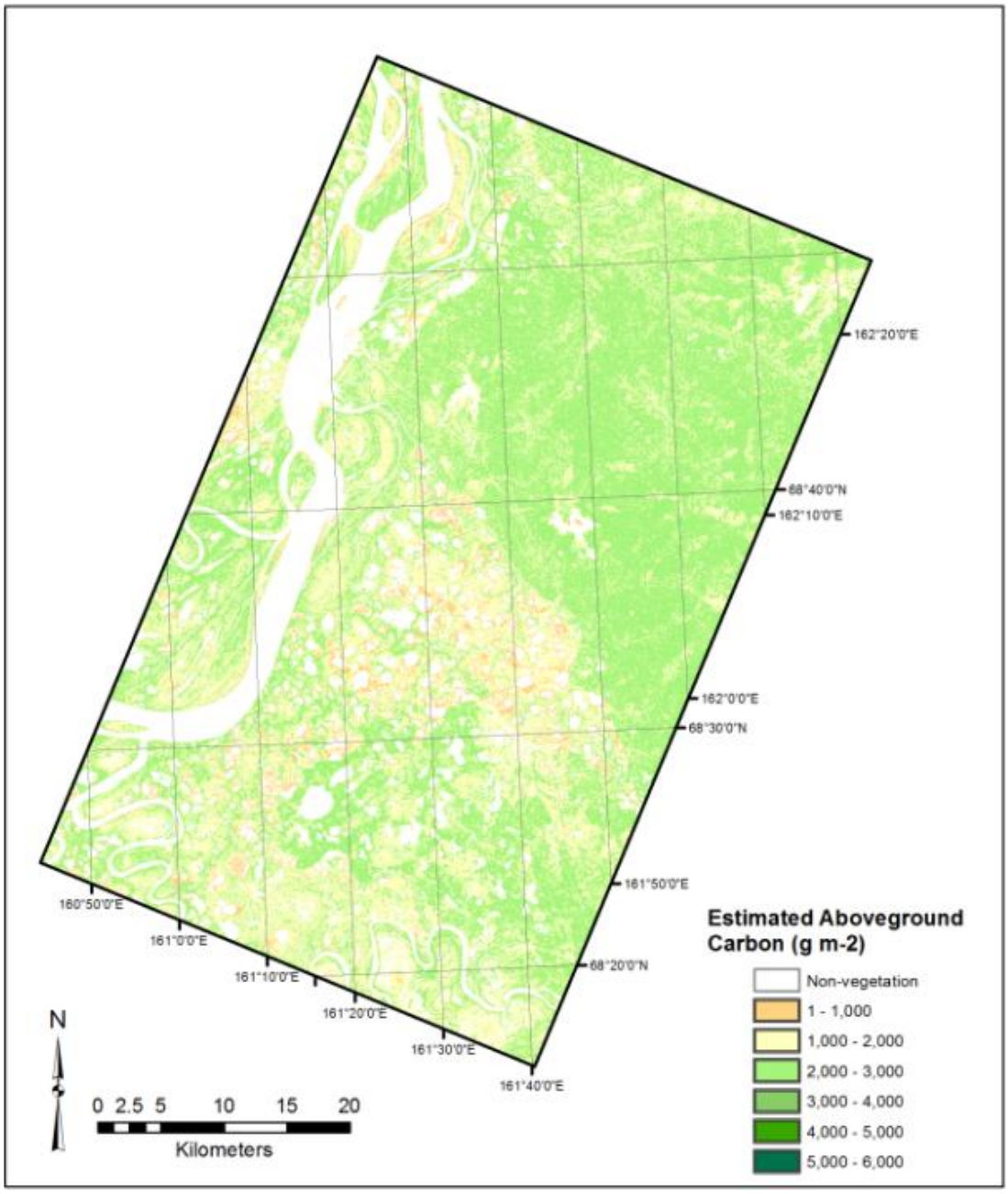

Figure 7b: Spectral mixture analysis output estimating the aboveground carbon in g m^{-2} based on the relative proportion of floodplain, larch, and shrubland and the measured carbon content associated with each.

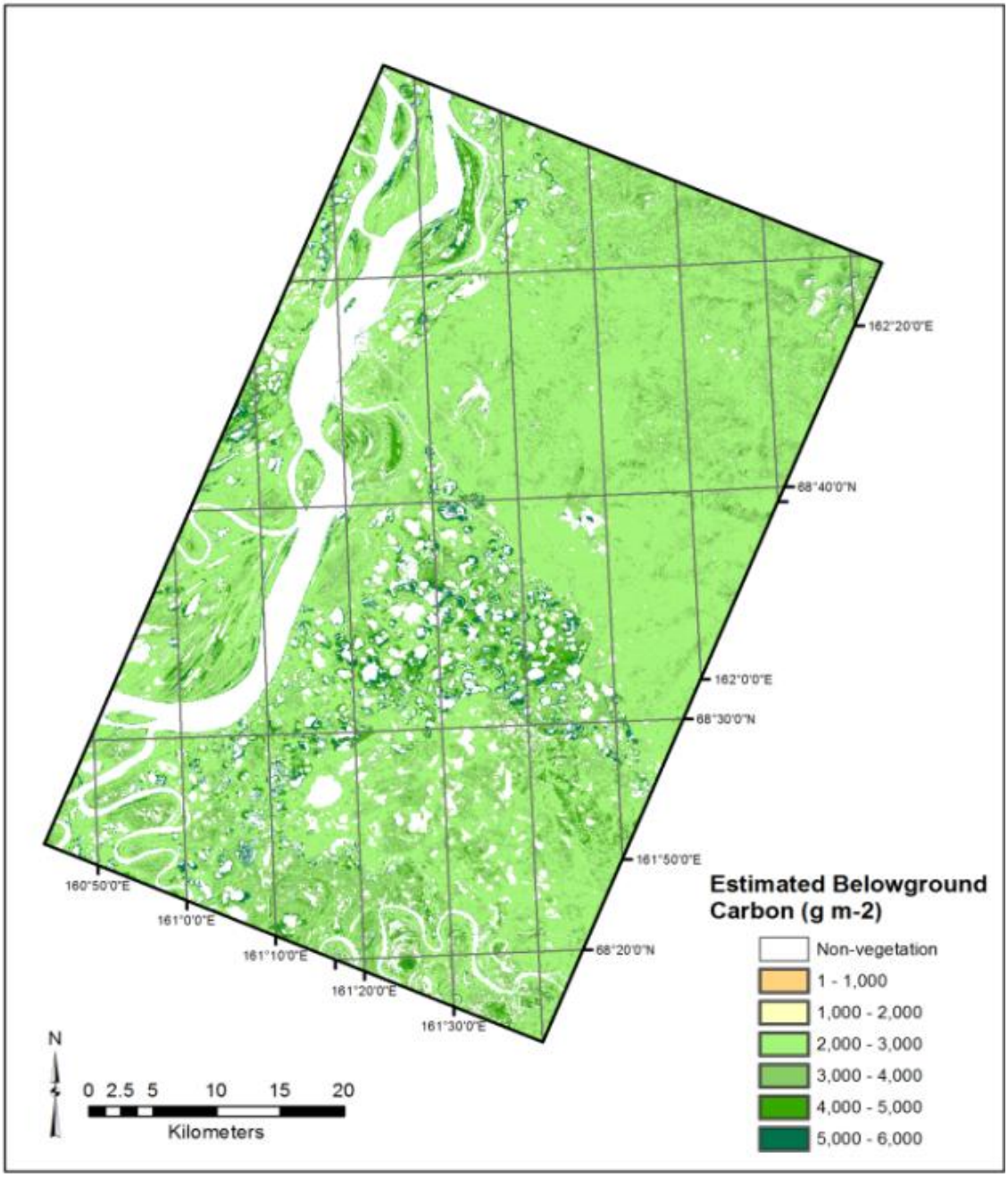

Figure 7: Spectral mixture analysis output estimating the belowground carbon in g m^{-2} based on the relative proportion of floodplain, larch, and shrubland and the measured carbon content associated with each.

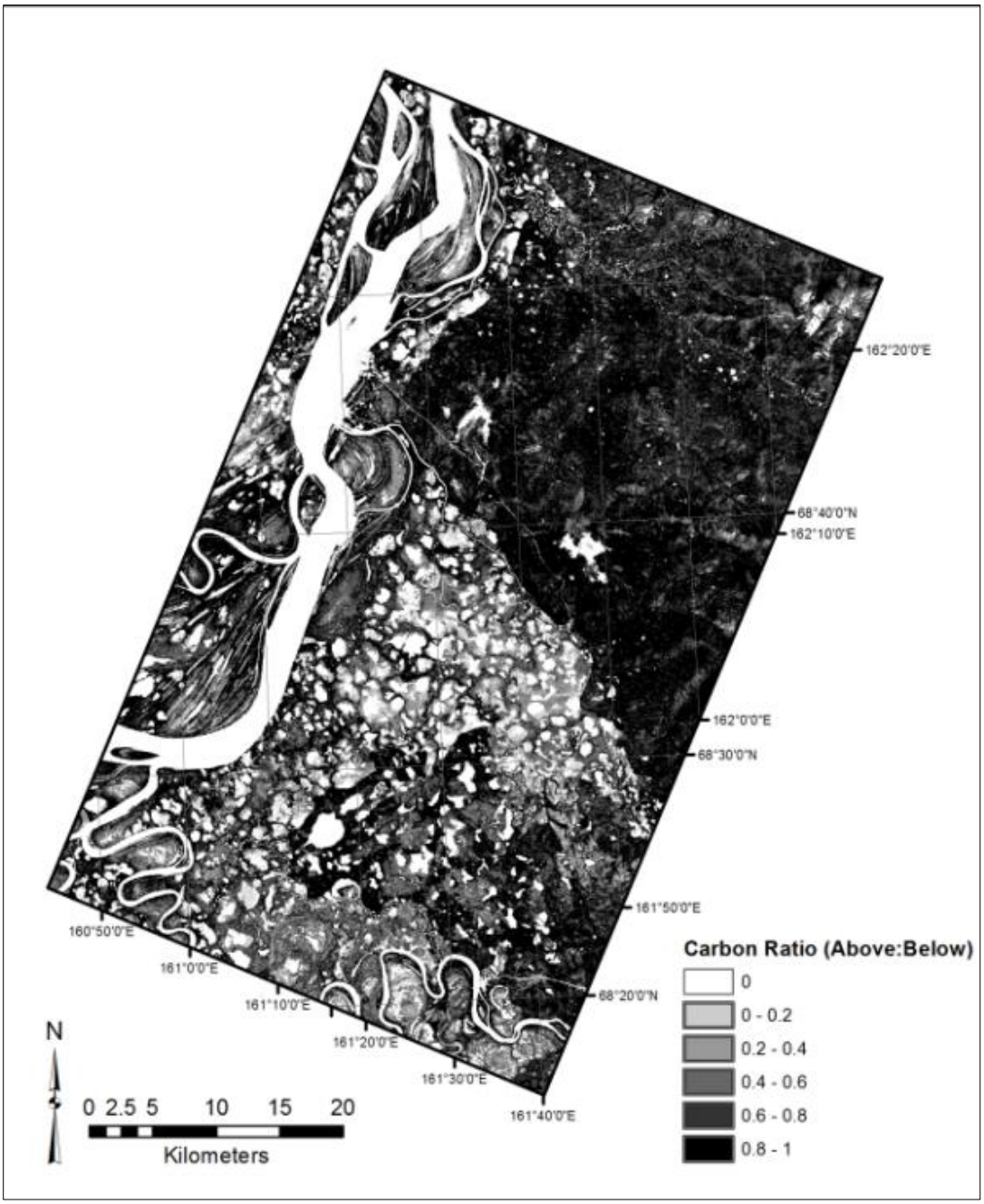

Figure 7d: Above to belowground carbon ratio based on spectral mixture analysis outputs estimating aboveground and belowground carbon in g m^{-2}.

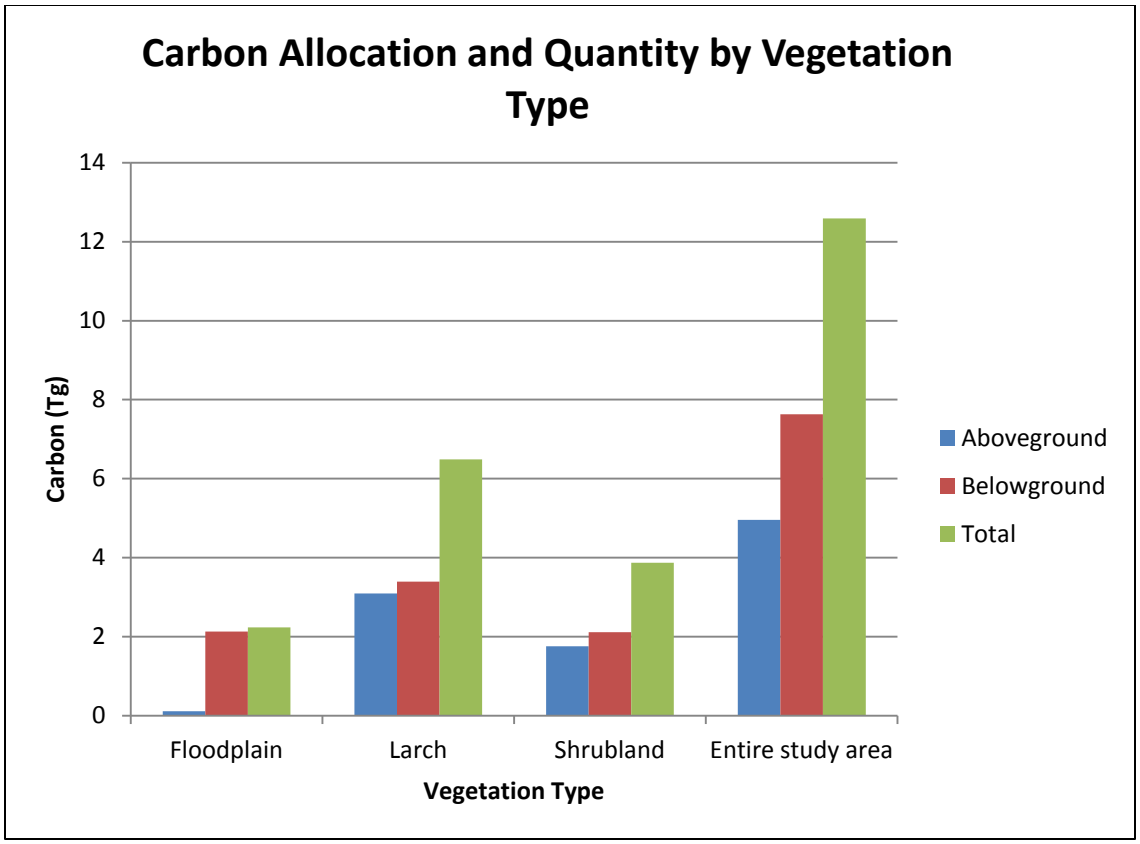

Figure 8: Summary of the carbon allocation and quantity by vegetation type for the entire study area.